Solution-Processable and Thermally Cross-Linkable Fluorene-Cored Triple-Triphenylamines with Terminal Vinyl Groups to Enhance Electroluminescence of MEH-PPV: Synthesis, Curing, and Optoelectronic Properties

Chia-Shing Wu, Ya-Ju Yang, Szu-Wen Fang, Yun Chen

Department of Chemical Engineering, National Cheng Kung University, Tainan 701, Taiwan
Correspondence to: Y. Chen (E-mail: yunchen@mail.ncku.edu.tw)

Received 16 March 2012; accepted 12 May 2012; published online
DOI: 10.1002/pola.26184

ABSTRACT: This study reports the synthesis, curing, and optoelectronic properties of a solution-processable, thermally cross-linkable electron- and hole-blocking material containing fluorene-core and three periphery *N*-phenyl-*N*-(4-vinylphenyl)benzeneamine (**FTV**). The **FTV** exhibited good thermal stability with T_d above 478 °C in nitrogen atmosphere. The **FTV** is readily cross-linked via terminal vinyl groups by heating at 160 °C for 30 min to obtain homogeneous film with excellent solvent resistance. Multilayer PLED device [ITO/PEDOT:PSS/cured-**FTV**/MEH-PPV/Ca (50 nm)/Al (100 nm)] was successfully fabricated using solution processed. Inserting cured-**FTV** is between PEDOT:PSS and MEH-PPV results in simultaneous reduction in hole injection from PEDOT:PSS to MEH-PPV and blocking in electron transport from MEH-PPV to anode. The maximum luminance and maximum current efficiency were enhanced from 1810 and 0.27 to 4640 cd/m^2 and 1.08 cd/A, respectively, after inserting cured-**FTV** layer. Current results demonstrate that the thermally cross-linkable **FTV** enhances not only device efficiency but also film homogeneity after thermal curing. **FTV** is a promising electron- and hole-blocking material applicable for the fabrication of multilayer PLEDs based on PPV derivatives. © 2012 Wiley Periodicals, Inc. J Polym Sci Part A: Polym Chem 000: 000–000, 2012

KEYWORDS: cross-linkable; flourene; luminescence; light-emitting diodes (LED); triphenylamine; vinyl

INTRODUCTION Since the discovery of green-yellow electroluminescence (EL) of poly(*p*-phenylene vinylene) (PPV) by Holmes et al. in 1990,[1] polymeric light-emitting diodes (PLEDs) continue to attract intensive interests because of their potential applications in large-area display and solid-state lighting.[2] In general, polymeric materials possess many advantages over inorganic ones, such as facile fabrication via spin-coating, roll-to-roll processing and other printing methods,[3,4] and susceptible to structural modification. However, for conventional electroluminescent {poly[2-methoxy-5-(2′-ethylhexyloxy)-1,4-phenylenevinylene]} MEH-PPV, holes are more readily injected and transported than electrons, leading to unbalanced carriers currents in PLEDs.[5–9] Maintaining a balance between electron and hole currents in PLEDs is an important factor for achieving high device efficiency. Various methods have been attempted to improve the device efficiency. One is to insert an additional electron injection/transport layer between the emitter and the cathode or an additional hole injection/transport layer between the emitter and the anode.[10–12] Nevertheless, fabrication of the multilayer polymer LEDs is usually a difficult task, such as one layer might be redissolved during subsequent spin-coating of next layer.

To prevent the drawback of redissolution during subsequent spin-coating, another method is developed high solvent resistance of polymers to increase their cross-linking density, which can be attained by photoexcited[13–15] or thermal[16–19] reactions. Therefore, many research groups prepared thermally cross-linkable polymers to be fabricated multilayer polymer LEDs in an attempt to balance charge injection/transport and then improve device performance. For instance, Jen and coworkers synthesized a series of highly efficient hole-transporting polymers with triphenylamine (TPA) or *N*,*N*′-bis(4-butylphenyl)-*N*,*N*′-diphenyl-1,1′-diphenyl-4,4′-diamine (di-Bu-TPD) covalently attached, as side chain, on the perfluorocyclobutane (PFCB) backbone to achieve an efficient blue light-emitting PLED (external quantum efficiency: 0.82%).[16] Reynolds and coworkers reported a novel AB2-type TPA to synthesize a hyperbranched polymer with subsequently polymerizable vinyl groups at the periphery as hole-transporting materials to fabricate multilayer polymer LEDs.[17(b)] Heeger and coworkers designed a thermally

Additional Supporting Information may be found in the online version of this article.

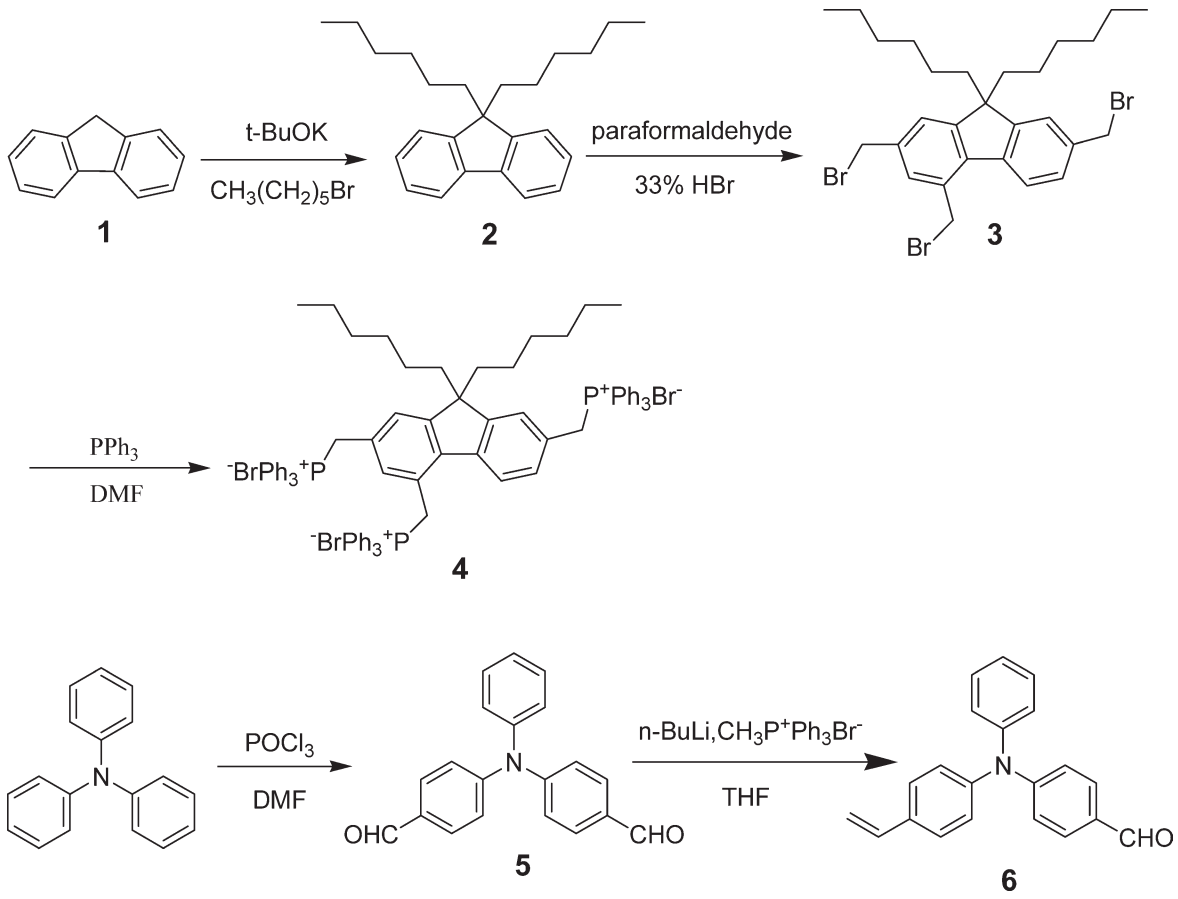

SCHEME 1 Synthesis of monomers **4** and **6**.

curable arylamine containing a PFCB structure as a hole-transporting polymer to enhance the current efficiency from 0.091 to 0.132 cd/A.[19(a)]

Among the typical fluorescent materials, fluorene-based derivatives show good thermal stability,[20–22] and the emission spectrum of fluorene derivatives overlaps partially with the absorption spectrum of MEH-PPV to facilitate energy transfer between them. TPA and its derivatives have attracted considerable interest as hole transport materials for use in organic EL devices.[23] However, the highest occupied molecular orbital (HOMO) level of TPA (−5.30 eV) is lower than that of MEH-PPV (−5.02 eV) to form the hole-blocking effect, whereas the lowest unoccupied molecular orbital (LUMO) level (−2.12 eV) is higher than that of MEH-PPV (−2.70 eV) to induce the electron-blocking effect.[24] TPA derivatives are inserted between PEDOT:PSS and MEH-PPV, which lead to more balanced charges recombination in the MEH-PPV emitting layer because of holes are usually more readily transported than electrons in MEH-PPV.

In this study, to more balanced charges recombination in the MEH-PPV, we synthesize a thermally cross-linking electron- and hole-blocking material containing triple TPAs with terminal vinyl groups 4,4′4′′-{[9,9-bis(hexyl)-9*H*-fluorene-2,4,7-triyl]tri-2,1-ethenediyl}tris{(*N*-phenyl-*N*-(4-vinyl phenyl)}benzeneamine (**FTV**). The **FTV** exhibits not only good thermal stability but also is readily cross-linked via vinyl groups by heating to obtain homogeneous film with excellent solvent resistance. The **FTV** is inserted via spin-coating and thermally cured between PEDOT:PSS and MEH-PPV to enhance both maximum luminance and maximum luminance efficiency of MEH-PPV. The results reveal that thermally cross-linkable fluorene-bridged triple-TPA with terminal vinyl groups (**FTV**) is applicable to enhance emission efficiency of MEH-PPV-based devices.

RESULTS AND DISCUSSION

Characterization of Thermally Cross-linkable Monomer (FTV)

Scheme 2 illustrates the synthetic routes used in the preparation of novel thermally cross-linkable monomer **FTV**. 2,4,7-Tris[methylene(triphenylphosphonium bromide)]-9,9-dihexyl fluorene (**4**) and 4-(phenyl(4-vinylphenyl)amino)benzaldehyde (**6**) were prepared successfully according to the procedures reported previously[25] (Scheme 1). Figure S2 (Supporting Information) shows the ^{1}H NMR, H-H COSY, ^{13}C NMR, and DEPT135 spectra of **FTV**. Assignments of each carbon and proton were assisted by the NMR spectra, and the structure of **FTV** was also confirmed via FT-IR, elemental analysis (EA), and mass spectrometry, which agree well with the proposed molecular structure of **FTV**. The chemical shifts at

TABLE 1 Thermal Properties of Thermally Cross-linkable **FTV**

Compound	T_d[a] (°C)	T_m[b] (°C)	ΔH[c] (J/g)	ΔH_{160}[d] (J/g)
FTV	478	91	−56.4	−58.1

[a] T_d, The decomposition temperature at 5 wt % loss was measured by TGA at a heating rate of 10 °C/min under nitrogen atmosphere.
[b] T_m, Melting point determined by DSC measurement.
[c] ΔH, Enthalpy of cross-linking in the first heating scan a heating rate of 10 °C/min.
[d] ΔH_{160}, Enthalpy of isothermal cross-linking at 160 °C within 30 min.

7.87–7.86 ppm (a) and 7.82–7.79 ppm (b) have been assigned to aromatic protons of fluorene and vinylene protons between fluorene and TPA moieties, respectively. The characteristic chemical shifts at 6.73–6.66 ppm (h), 5.69–5.65 ppm (i), and 5.19–5.16 ppm (j) indicate the existence of terminal vinyl groups from which thermally cross-linkable character can be expected (Fig. S2a). The **FTV** is soluble in common organic solvents such as toluene, THF, chloroform, and chlorobenzene.

Thermal Cross-linking and Thermal Resistant Properties

Thermal cross-linking and thermal resistant characteristics of **FTV** were studied by differential scanning calorimeter (DSC) and (thermogravimetric analysis) TGA, respectively. The thermal decomposition temperature (T_d) of **FTV** was about 478 °C and its residual weight (at 900 °C) was above 40% under nitrogen atmosphere, indicating their highly thermal stability (Fig. S3, Supporting Information; Table 1). Thermal cross-linking reaction characteristics of **FTV** were first investigated by two DSC heating scans from 30 to 250 °C at a rate of 10 °C/min. In the first scan, the DSC trace showed a melting temperature (T_m) at 91 °C and an exothermic peak at 160 °C in which the exotherm started at about 130 °C (Fig. 1). The joule heat released (56.4 J/g) is due to thermal cross-linking reaction of the terminal vinyl groups. Nevertheless, no apparently detectable exothermic peak is observed upon the second heating, suggesting that most of the terminal vinyl groups have been reacted during the first heating scan. Moreover, the cured **FTV** shows no obviously detectable glass transition and melting temperatures up to 220 °C, indicating that it would be basically an amorphous material. Highly thermal stability is desirable of cured **FTV** to prevent its crystallization during device operation or thermal treatment. As shown in Figure 2, the exothermic thermal cross-linking of **FTV** under 160 °C is completed within 30 min. The joule heat released (58.1 J/g) is very close to that obtained for the first heat scanning (56.4 J/g). This can be confirmed by the absence of exothermic peak in the DSC trace of the thermally cross-linked sample. To ensure complete cross-linking in the following study, the thermal treatment of **FTV** films was conducted at 160 °C for 30 min.

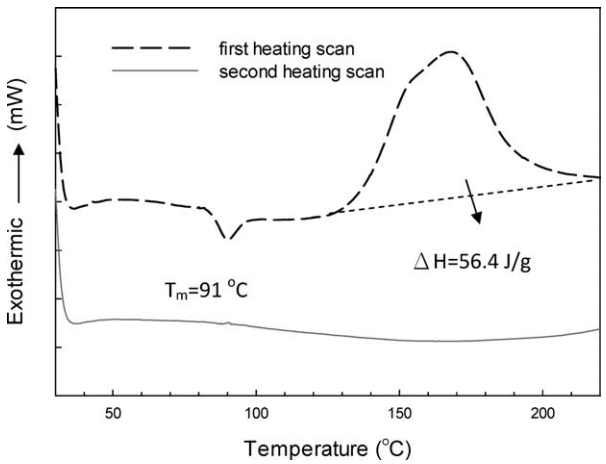

FIGURE 1 Differential scanning calorimetric curves of **FTV** at a heating rate of 10 °C/min under nitrogen atmosphere. The first run was used to observe the reaction heat of periphery or terminal vinyl groups of **FTV**.

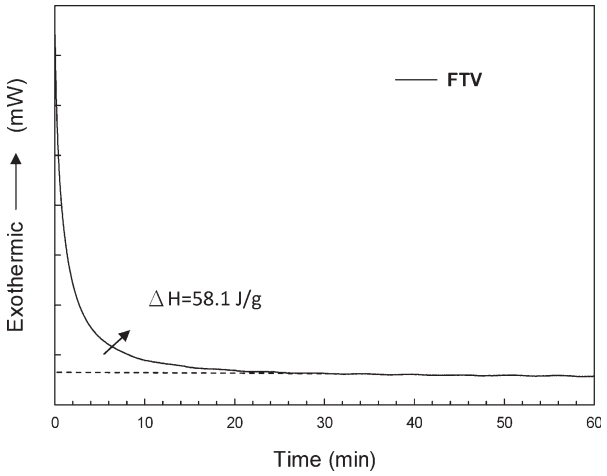

FIGURE 2 Isothermal DSC traces of **FTV** at 160 °C under nitrogen atmosphere.

Photophysical and Solvent Resistant Properties

Figure 3 illustrates the absorption and photoluminescence (PL) spectra of monomer **FTV** in solution ($CHCl_3$) and as films spin-coated from $CHCl_3$ solution with the characteristic optical data summarized in Table 2. The absorption

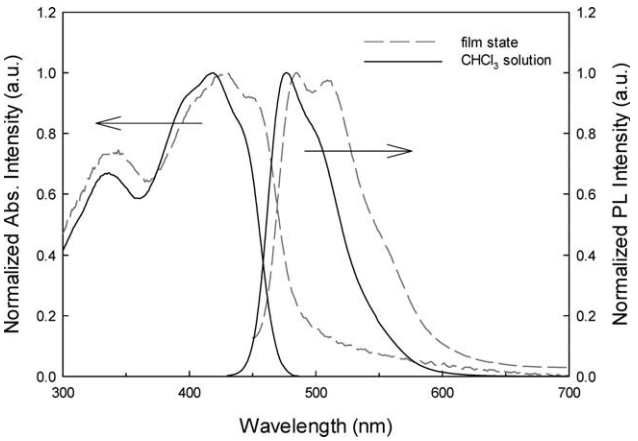

FIGURE 3 UV-vis absorption and photoluminescence spectra of **FTV** in $CHCl_3$ solution (λ_{ex} = 419 nm) and film state (λ_{ex} = 429 nm).

TABLE 2 Optical Properties of **FTV** in $CHCl_3$ Solution and Film State

	Solution[a]		Film	
	UV-vis λ_{max}[a] (nm)	PL λ_{max}[a] (nm)	UV–vis λ_{max} (nm)	PL λ_{max} (nm)
FTV	336, 419	477, 501	339, 429	485, 509

[a] In chloroform (1×10^{-5} M).

maximum peaks of monomer **FTV** in $CHCl_3$ and as films appear at about 419 nm (with shoulder at 336 nm) and 429 nm (with a shoulder at 339 nm), respectively. The major absorption of **FTV** (ca. 419 nm and 429 nm) can be attributed to the π–π^* transitions of their conjugated flourene core, whereas the shorter-wavelength absorption (ca. 336 nm and 339 nm) is definitely originated from terminal TPA moieties. The major PL spectra of **FTV** in solution and solid state locate at about 477 nm (with shoulder at 501 nm) and about 485 nm (with large shoulder at 509 nm), respectively. Solid state absorption and PL maxima of **FTV** are slightly red-shifted (3–10 nm and 8 nm) relative to solution state, probably due to aggregate formation via intra- or interchain interactions.

Highly resistant to solvents is necessary for the fabrication of multilayer PLEDs by solution processes. Solvent resistance of the thermally cross-linked **FTV** film at 160 °C for 30 min was investigated by the absorption spectra before and after spin-coating with chlorobenzene which is a good solvent for the uncured film. As shown in Figure S4 (Supporting Information), the absorption spectrum of the pristine **FTV** film almost disappears after chlorobenzene spin-coating, implying that the **FTV** film is readily dissolved out during the solution-coating process. However, the absorption spectral intensity of the thermally cross-linked **FTV** film reduces only slightly after the spin-coating (Fig. 4). In addition, the FTIR spectral variations of the pristine **FTV** film and the thermally

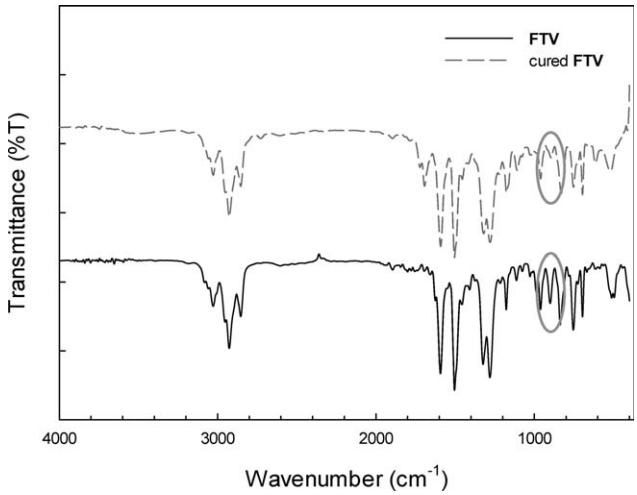

FIGURE 5 FTIR spectra of **FTV** (——) and cured-**FTV** (– – –). The cured-**FTV** was obtained by treating at 160 °C for 30 min under nitrogen atmosphere.

cross-linked **FTV** film were also investigated. The intensity of characteristic absorption of terminal vinyl groups (ca. 900 cm^{-1}) diminishes dramatically after thermal cross-linking (Fig. 5). Therefore, the high solvent resistance of cured **FTV** is attributed to its increased cross-linking density after the thermal curing.

Electrochemical Investigations

Cyclic voltammetry was used to investigate the electrochemical properties of pristine **FTV** and thermally cross-linked **FTV**. Pristine- and cured-**FTV**-coated ITO glasses were used as the working electrode, immersed in anhydrous acetonitrile containing 0.1 M tetra-*n*-butylammonium perchlorate (Bu_4NClO_4) as electrolyte. Their HOMO energy levels were estimated by the equations: E_{HOMO} (eV) = - ($E_{ox,FOC}$ + 4.8), where $E_{ox,FOC}$ is the onset oxidation potentials, respectively, relative to the ferrocene/ferrocenium couple whose energy level is already known (−4.8 eV). Their LUMO energy levels

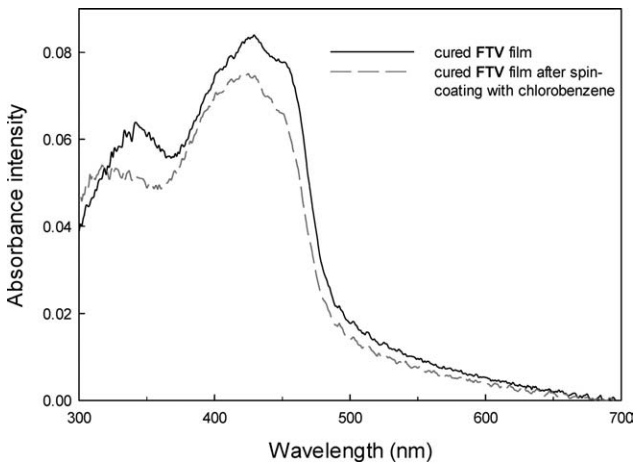

FIGURE 4 Absorption spectra of cured **FTV** film (at 160 °C for 30 min under nitrogen atmosphere): before (——) and after (– – –) spin-coating with chlorobenzene.

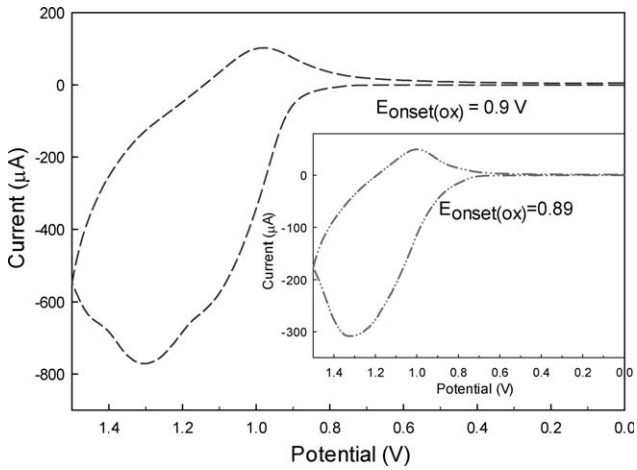

FIGURE 6 Cyclic voltammograms of **FTV** and cured-**FTV** (inset) coated on ITO glass as working electrode (scan rate: 100 mV/s).

TABLE 3 Electrochemical Properties of **FTV**

Monomer/ Polymer	$E_{onset(ox)}$ vs. FOC(V)[a]	E_{HOMO} (eV)[b]	E_{LUMO} (eV)[c]	E_g^{opt} (eV)[d]
FTV	0.40	−5.20	−2.64	2.56
Cured-**FTV**	0.39	−5.19	−2.64	2.55

[a] E_{FOC}= 0.50 V vs. Ag/AgCl.
[b] $E_{HOMO} = -e(E_{onset(ox),\ FOC} + 4.8\ V)$.
[c] $E_{LUMO} = -e(E_{HOMO} + E_g^{opt})$.
[d] Band-gaps estimated from onset absorption (λ_{onset}): $E_g^{opt} = 1240/\lambda_{onset}$.

were calculated by $E_{LUMO} = -e(E_{HOMO} + E_g^{opt})$, where the optical band-gap (E_g^{opt}) was estimated from onset absorption. The cyclic voltammograms are shown in Figure 6, with the representative electrochemical data summarized in Table 3. The estimated HOMO energy levels of pristine and cured **FTV** are similar to be −5.20 and −5.19 eV, respectively, meaning that their electrochemical properties are almost not affected by terminal vinyl groups. The estimated LUMO energy levels of pristine and cured **FTV** are −2.64 eV using the HOMO levels and the optical band gap (E_g) calculated from onset absorption. Moreover, the HOMO energy levels of PEDOT:PSS, cured-**FTV**, and MEH-PPV are −5.0 eV, −5.19 eV, and −5.02 eV, respectively, whereas the LUMO energy levels of cured-**FTV** and MEH-PPV are −2.64 eV and −2.70 eV, respectively. The lower HOMO level of cured-**FTV** (−5.19 eV) than MEH-PPV (−5.02 eV) result in blocking of holes, whereas the higher LUMO level (−2.64 eV) than MEH-PPV (−2.70 eV) induces electron-blocking effect.[24] Therefore, the cured-**FTV** can be inserted between PEDOT:PSS and MEH-PPV to simultaneously reduce hole injection from PEDOT:PSS to MEH-PPV and to block electron transport from MEH-PPV to anode. Accordingly, this might be an effective strategy to balance charges recombination in the MEH-PPV emitting layer whose holes are usually more readily transported than electrons.

Performance Enhancement of MEH-PPV by Thermally Cross-linkable FTV

According to the energy band diagrams depicted in Figure 7, the energy barrier between Calcium (Ca) and MEH-PPV (0.20 eV) is higher than that between PEDOT:PSS and MEH-PPV (0.02 eV). Moreover, holes are usually more readily transported than electrons in MEH-PPV. These two effects will result in reduced recombination ratio of holes and electrons. The imbalance of charges transport in MEH-PPV can be mitigated by inserting cured-**FTV** between PEDOT:PSS and MEH-PPV layers to reduce hole injection from PEDOT:PSS to MEH-PPV and to block electron transport from MEH-PPV to anode simultaneously. For this reason, cured-**FTV** was inserted between PEDOT:PSS and MEH-PPV to solve MEH-PPVs common defect of unbalanced charges transport, and multilayer PLEDs [ITO/PEDOT:PSS/cured-**FTV** (or not)/MEH-PPV/Ca (50 nm)/Al (100 nm)] were fabricated via successive spin-coating processes to investigate their device performances.

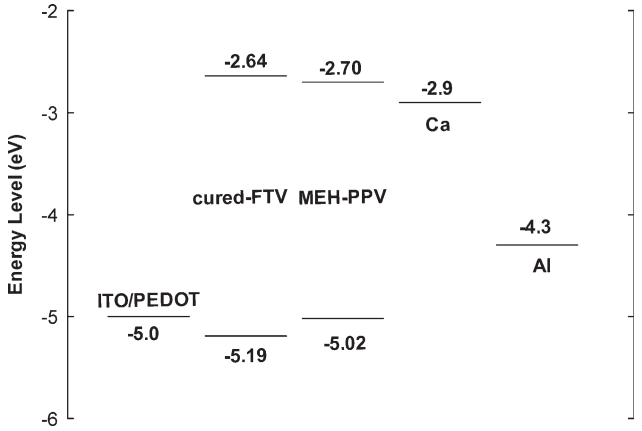

FIGURE 7 Energy band diagrams of PEDOT:PSS, cured-**FTV**, MEH-PPV, and cathode.

Figure 8 shows the current density and luminance versus bias characteristics of the multilayer devices, with the corresponding performance data summarized in Table 4. The turn-on voltages are slightly increased to 3.6 V from 3.1 V of the device without cured-**FTV** layer. This is probably attributable to hole-blocking effect of the cured-**FTV** layer that extra bias is needed to turn on the multilayer device.[26] Moreover, maximum luminance and maximum current efficiency are enhanced from 1810 and 0.27 to 4640 cd/m^2 and 1.08 cd/A, respectively, by adding cured-**FTV** layer (film thickness: 55 ± 5 nm) (Fig. 8; Table 4). The device performance enhancement results from more balanced charges injection and transport by inserting thermally cross-linked **FTV**. However, further increase in cured-**FTV** layer thickness leads to degradation in maximum luminance and maximum current efficiency; i.e., diminish to 1880 cd/m^2 and 0.58 cd/A, respectively, with cured-**FTV** (90 ± 5 nm). This performance degradation is probably due to more hole-blocking effect to result in imbalance of charge injection and transport with higher film thicknesses of cured-**FTV**. Therefore, the

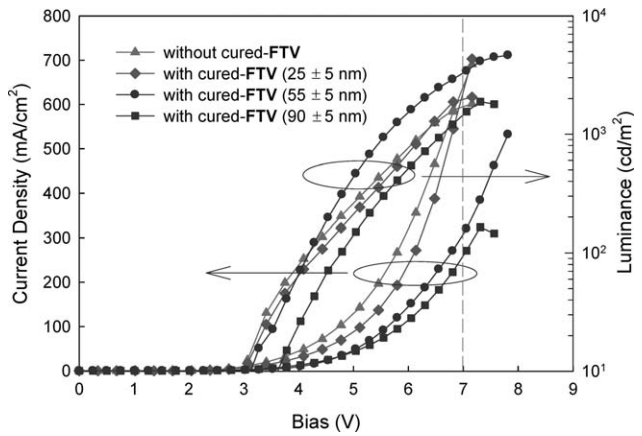

FIGURE 8 Current density versus bias and luminance versus bias characteristics of PLEDs without or with cured-**FTV** layers. Device configuration: ITO/PEDOT:PSS/(cured-**FTV**)/MEH-PPV/Ca (50 nm)/Al (100 nm).

TABLE 4 Optoelectronic Properties of the Light-emitting Diodes[a]

Cured-**FTV** layer	Turn-on voltage (V)[b]	L_{max} (cd/m^2)[c]	LE_{max} (cd/A)[d]	Emission (λ_{em}, nm)[e]	CIE Coordinates (x, y)[f]
Non	3.1	1810	0.27	580, 626	(0.57, 0.43)
cured-**FTV** (25 ± 5 nm)	3.1	2060	0.34	580, 626	(0.57, 0.43)
cured-**FTV** (55 ± 5 nm)	3.2	4640	1.08	575, 625	(0.54, 0.46)
cured-**FTV** (90 ± 5 nm)	3.6	1880	0.58	586, 625	(0.59, 0.41)

[a] Device structure: ITO/PEDOT:PSS/cured-**FTV** or not/MEH-PPV/Ca(50nm) /Al(100 nm).
[b] Turn-on voltage at about 10 cd/m^2.
[c] Maximum luminance.
[d] Maximum luminance efficiency.
[e] Electroluminescent spectra at maximum luminance.
[f] The 1931 CIE coordinate at maximum luminance.

appropriate film thickness of cured-**FTV** was benefit to enhance the device performance of MEH-PPV.

Current density versus bias curve shifts horizontally to higher bias after inserting cured-**FTV** layer (Fig. 8). The horizontal shift suggests that the current density is reduced under the same operating bias. For instance, at operating bias of 7 V the current density decreases from 700 to 280 mA/cm^2, which is probably due to increased hole blocking by cured-**FTV** layer (Fig. 8). The hole-blocking effect reduces hole injection from PEDOT:PSS to MEH-PPV solving the common defect of MEH-PPV in which holes are usually more readily transported than electrons. At the same time, the cured-**FTV** slightly blocks electrons to avoid quenching in anode due to its higher LUMO energy levels (−2.64 eV) than MEH-PPV (−2.70 eV) (Fig. 7). Moreover, a hole-only device [ITO/PEDOT:PSS/cured-**FTV** (60 nm)/Au (20 nm)/Al (100 nm)] was fabricated to investigate the hole mobility (Fig. S5, Supporting Information). Estimated hole mobility of the cured-**FTV** film (film thickness: 60 nm) was about 4.42×10^{-6} cm^2/Vs at 11.8×10^5 V/cm, using the space charge limited current model.[27] This holy mobility is smaller than about 10^{-5} cm^2/Vs of conventional MEH-PPV.[28] Therefore, more balanced charges injection and transport in MEH-PPV is attained by inserting thermally cross-linked **FTV** between PEDOT:PSS and MEH-PPV layers.

In addition, the morphology of pristine and cured-**FTV** were also investigated by atomic force microscope (AFM) to investigate the effect of thermal treatment. As shown in Figure 9, the surface homogeneity of cured-**FTV** (RMS roughness: 1.09 nm) is superior to than that of pristine **FTV** (RMS roughness: 1.94 nm). Homogeneous surface morphology is advantageous to enhance device performance. Figure 10 shows the electroluminescent emissions of the devices are exclusively originated from MEH-PPV, with full width at half-maxima (fwhm) being about 70 nm (with cured-**FTV**) and 90 nm (without cured-**FTV**). Furthermore, the 1931 CIE coordinates (x, y) of the EL emission shift slightly from (0.57, 0.43) to (0.54, 0.46) and (0.59, 0.41) after inserting the cured-**FTV** layer. Consequently, through fabrication of multilayer device, solution-processable and thermally cross-linkable **FTV** is effective in enhancing device performance of the conventional MEH-PPV.

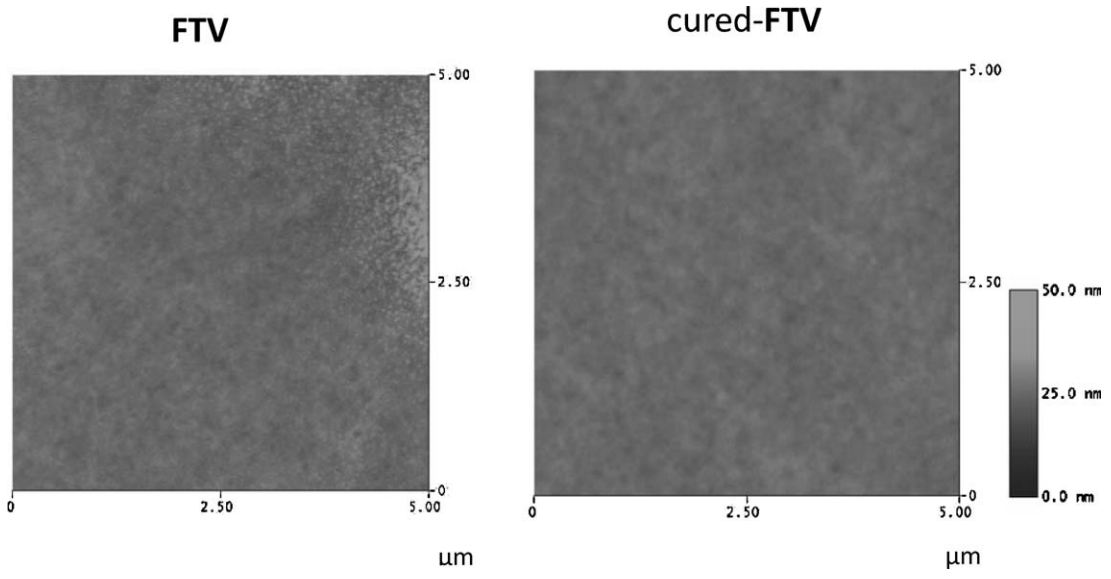

FIGURE 9 Surface AFM images of **FTV** and cured-**FTV** film coated on ITO glasses on tapping modes.

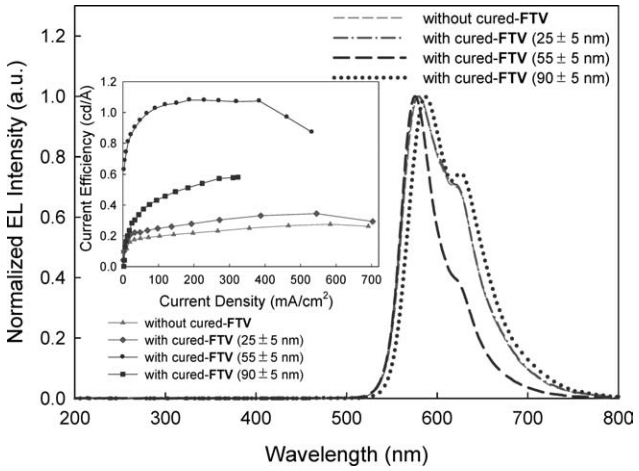

FIGURE 10 Emission spectra of PLEDs without or with cured-**FTV** layers. Device configuration: ITO/PEDOT:PSS/(cured-**FTV**)/MEH-PPV/Ca (50 nm)/Al (100 nm). Inset: current efficiency versus current density characteristics of PLEDs without or with cured-**FTV** layers.

EXPERIMENTAL

Measurements

Newly synthesized compounds were identified by NMR spectra, FT-IR spectra, and EA. ^{1}H NMR and ^{13}C NMR spectra were obtained on a Bruker AMX-400 MHz spectrometer, with the chemical shifts reported in ppm using tetramethylsilane as an internal standard. The FTIR spectra were measured as KBr disk on a Fourier transform infrared spectrometer, model 7850 from Jasco. Elemental analysis was carried out on a Heraus CHN-Rapid elemental analyzer. TGA of polymers was performed under nitrogen atmosphere at a heating rate of 15 °C/min using a PerkinElmer TGA-7 thermal analyzer. Thermal transition properties of polymers were investigated using a DSC, Mettler Toledo DSC 1 Star^{e} System, under nitrogen atmosphere at a heating rate of 10 °C/min. Absorption and PL spectra were measured with a Jasco V-550 spectrophotometer and a Hitachi F-4500 fluorescence spectrophotometer, respectively. Cyclic voltammograms were recorded with a voltammetric analyzer (model CV-50W from Bioanalytical Systems, Inc.) at room temperature under nitrogen atmosphere. The measuring cell was made up of a polymer-coated ITO glass as the working electrode, an Ag/AgCl electrode as the reference electrode, and a platinum wire as the auxiliary electrode. The electrodes were immersed in acetonitrile containing 0.1 M $(n\text{-Bu})_4NClO_4$ as electrolyte. The energy levels were calculated using ferrocene (FOC) as standard (−4.8 eV with respect to vacuum level).[29] An AFM, equipped with a Veeco/Digital Instrument Scanning Probe Microscope (tapping mode) and a Nanoscope IIIa controller, was used to examine the morphology and to estimate the thickness and root-mean-square roughness of deposited films.

Materials

Fluorene (Acros), 1-bromohexane (Acros), triphenylamine (Acros), (methyl)triphenyl phosphonium bromide (Acros), potassium *tert*-butoxide (*t*-BuOK, Lancaster), paraformaldehyde (Showa), hydrogen bromide solution (33 wt %) in glacial acetic acid (Acros), triphenylphosphine (Alfa Aesar), phosphous oxychloride (RDH), sodium hydroxide (J. T. Baker), *N*,*N*-dimethylformamide (DMF, Tedia), *n*-hexane (Tedia), toluene (Tedia), benzene (Fisher), chloroform (Tedia), ethanol (J. T. Baker), dichloromethane (Seedchem), and other solvents were of commercial sources and used without further purification. 2,4,7-tris[methylene(triphenylphosphonium bromide)]-9,9-dihexyl fluorene (**4**) was prepared from 9,9-dihexylfluorene (**2**) by reacting consecutively with paraformaldehyde, HBr aqueous solution (33 wt %), and triphenylphosphine. 4-(Phenyl(4-vinylphenyl)amino)benzaldehyde (**6**) was synthesized from 4,4′-(phenylazanediyl)dibenzaldehyde (**5**) by reacting with (methyl)triphenyl phosphonium bromide (Scheme 1).

Synthesis of Thermally Cross-linkable Monomer (FTV)

A mixture of 2,4,7-tris[methylene(triphenylphosphonium bromide)]-9,9-dihexyl fluorene (**4**: 1.33 g, 0.95 mmol) and 4-(phenyl(4-vinylphenyl)amino)benzaldehyde (**6**: 1.00 g, 3.34 mmol) in 30 mL of *N*,*N*-dimethylformamide was stirred at room temperature for 30 min (Scheme 2). It was added with sodium ethoxide (3.2 mL, 8.55 mmol) and stirred for additional 24 h under nitrogen atmosphere. After cooling to room temperature, the reaction mixture was precipitated from distilled water. The precipitated solid was collected by filtration, dried *in vacuo*, and purified by column chromatography (eluent: *n*-hexane/CH_2Cl_2 = 3/1). The concentrated yellow solid was redissolved in $CHCl_3$, precipitated from ethanol, and dried *in vacuo* to afford yellow 4,4′4″-{[9,9-bis(hexyl)-9H-fluorene-2,4,7-triyl]tri-2,1-ethenediyl}tris{(*N*-phenyl-*N*-(4-vinylphenyl)}benzeneamine (**FTV**) (43%). FTIR (KBr pellet, cm^{-1}): *v* 3028, 2925, 2854 (C—H stretching vibrations of aliphatic and aromatic), 1593, 1504 (—C=C—), 901 (—C=CH_2 out-of-plane). ^{1}H NMR ($CDCl_3$, 500 MHz): δ 7.87–7.86 (d, 1H, J = 6.6 Hz, Ar-H), 7.82–7.79 (d, 1H, J = 12.8 Hz), 7.64 (s, 1H), 7.56–7.55 (d, 2H, J = 6.9 Hz), 7.53 (s, 1H), 7.49–7.45 (m, 5H), 7.43 (s, 1H), 7.36–7.28 (m, 13H), 7.24–7.05(m, 26H), 6.73–6.66 (m, 3H, vinyl, CH), 5.69–5.65 (d, 3H, J = 17.6 Hz, vinyl, cis-CH), 5.19–5.16 (d, 3H, J = 10.8 Hz, vinyl, trans-CH), 2.07–2.03 (t, 4H, J = 8 Hz, —CH_2—), 1.15–1.03 (m, 12H, —CH_2—), 0.78–0.75 (t, 6H, J = 5.6 Hz, —CH_3),0.71–0.64 (m, 4H, —CH_2—) ppm. ^{13}C NMR (CD_2Cl_2, 400 MHz): δ 152.95, 152.70, 147.90, 147.77, 141.85, 138.24, 137.01, 136.75, 134.47, 132.87, 132.54, 131.41, 129.93, 129.91, 128.17, 127.87, 127.67, 127.65, 126.22, 126.00, 125.39, 125.35, 124.55, 124.52, 124.36, 124.32, 123.99, 123.93, 120.84, 119.72, 112.68, 41.43, 32.12, 30.30, 23.18, 14.35 ppm. FAB-MS (m/z): calcd: 1219.67; Found: 1222.00. Anal. Calcd. (%) for $C_{91}H_{85}N_3$: C, 89.54; H, 7.02; N, 3.44. Found: C, 89.45; H, 7.09; N, 3.36.

Fabrication of Multilayer Polymer Light-emitting Diodes via Solution-Process

Multilayer polymer light-emitting diodes (ITO/PEDOT:PSS/thermal cross-linkable **FTV**/polymer/Ca/Al) were fabricated to investigate their optoelectronic characteristics. Transparent indium tin oxide (ITO) glass was successively cleaned

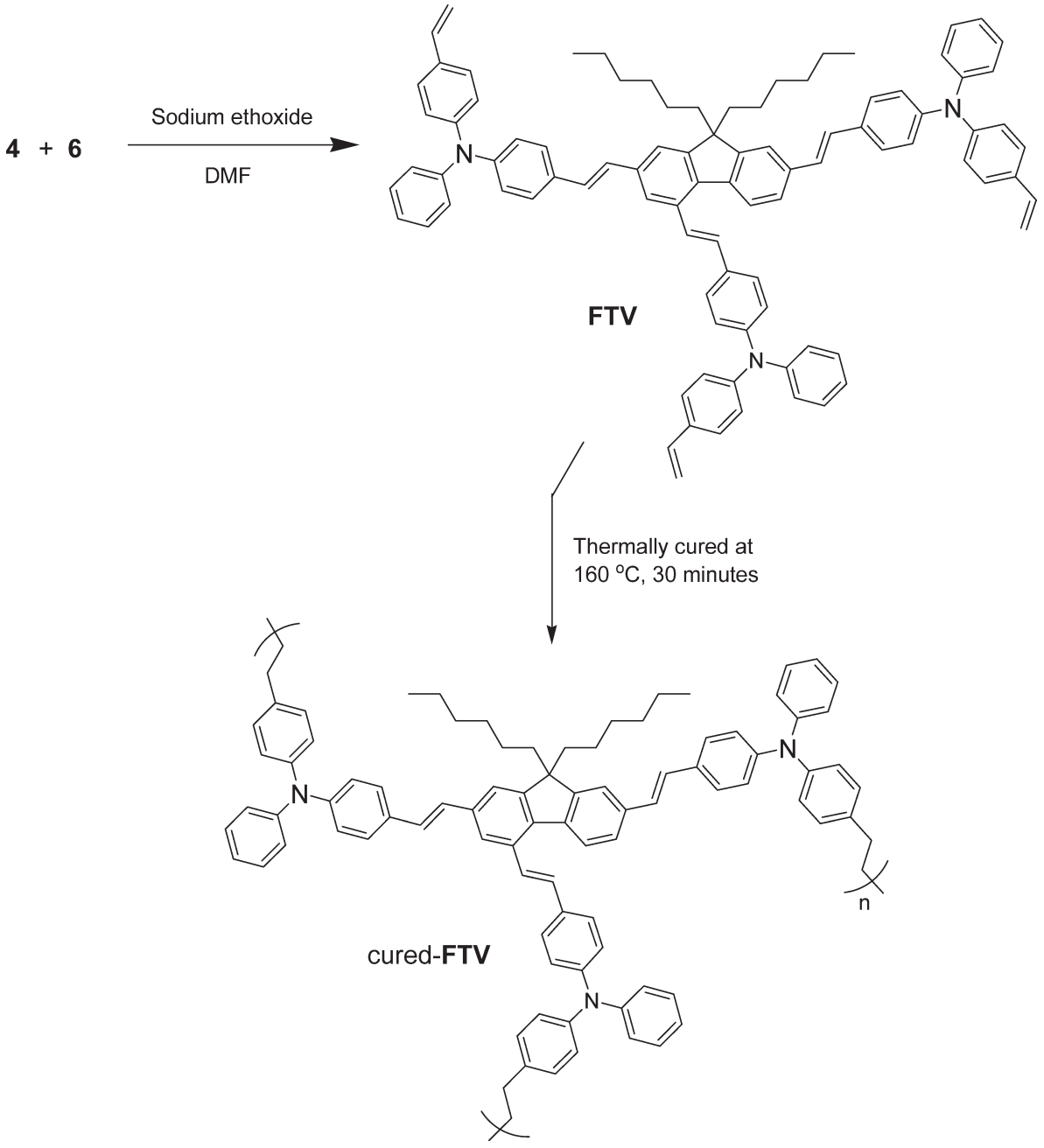

SCHEME 2 Synthesis of thermally cross-linkable monomer **FTV** and cured-**FTV**.

with neutraler reiniger/deionized water (1/3 = v/v) mixture, deionized water, acetone and 2-propanol, and then dried *in vacuo* overnight. Aqueous dispersion of PEDOT:PSS was spin-coated on top of the cleaned ITO glass as hole-injection layer and dried at 150 °C for 15 min. Thermal cross-linkable **FTV** was then deposited by spin-coating (2000 rpm) onto the PEDOT:PSS layer from a polymer solution in chlorobenzene (5 mg/mL) and then cross-linked at 160 °C for 30 min. Emitting layer was then deposited by spin-coating (2000 rpm) onto the cured **FTV** layer from a polymer solution (MEH-PPV) in chlorobenzene (10 mg/mL). Finally, calcium and aluminum were consecutively vacuum-deposited as cathode using a vacuum coater at a pressure of 2×10^{-6} Torr. Luminance versus voltage and current density versus voltage characteristics of the devices were measured using a combination of a Keithley power source (model 2400) and an Ocean Optics usb2000 fluorescence spectrophotometer. The optoelectronic measurements were conducted in a glove-box filled with nitrogen.

CONCLUSIONS

We have successfully synthesized and characterized a thermally cross-linkable electron- and hole-blocking **FTV**

containing fluorene-core and three *N*-phenyl-*N*-(4-vinylphenyl)benzeneamine terminals. The **FTV** was soluble in common organic solvents and thermally stable (T_d at 5 wt % loss: 478 °C and residual weight: above 40% at 900 °C). The **FTV** revealed excellent solvent resistance and moderate film morphology (RMS roughness = 1.09 nm) after thermal cross-linking at 160 °C for 30 min. The photophysical and electrochemical properties of cured-**FTV** remain almost unchanged compared to pristine **FTV**. The HOMO energy level of cured-**FTV** (−5.19 eV) is lower than those of PEDOT:PSS (−5.0 eV) and MEH-PPV (−5.02 eV), whereas the LUMO energy level of cured-**FTV** (−2.64 eV) is slightly higher than that of MEH-PPV (−2.70 eV). Inserting cured-**FTV** between PEDOT:PSS and MEH-PPV layers to simultaneously reduction of hole injection from PEDOT:PSS to MEH-PPV and blocking of electron transport from MEH-PPV to anode. The device performance was significantly enhanced, by inserting cured-**FTV**, due to more balanced charges recombination in MEH-PPV. The multilayer device with cured-**FTV** showed maximum luminance of 4640 cd/m^2 and maximum current efficiency of 1.08 cd/A. Current results indicate that the solution-processable and thermally cross-linkable **FTV** is a promising electron- and hole-blocking layer for the performance improvement of MEH-PPV or other PPV-based devices.

ACKNOWLEDGMENTS

The authors thank the National Science Council of Taiwan for financial aid through project NSC 98-2221-E-006-002-MY3.

REFERENCES AND NOTES

1 Burroughes, J. H.; Bradley, D. D. C.; Brown, A. R.; Marks, R. N.; Mackay, K.; Friend, R. H.; Burn, P. L.; Holmes, A. B. *Nature* **1990,** *347*, 539–541.

2 (a) Grem, G.; Leditzky, G.; Ullrich, B.; Leising, G. *Adv. Mater.* **1992,** *4*, 36–37; (b) Pei, Q.; Yang, Y. *J. Am. Chem. Soc.* **1996,** *118*, 7416–7417; (c) Andersson, M. R.; Thomas, O.; Mammo, W.; Svensson, M.; Theander, M.; Inganäs, O. *J. Mater. Chem.* **1999,** *9*, 1933–1940.

3 (a) Aguiar, M.; Karasz, F. E.; Akcelrud, L. *Macromolecules* **1995,** *28*, 4598–4602; (b) Kolb, E. S.; Gaudiana, R. A.; Mehta, P. G. *Macromolecules* **1996,** *29*, 2359–2364; (c) Kraft, A.; Grimsdale, A. C.; Holmes, A. B. *Angew Chem. Int. Ed.* **1998,** *37*, 402–428.

4 (a) Friend, R. H.; Gymer, R. W.; Holmes, A. B.; Burroughes, J. H.; Marks, R. N.; Taliani, C.; Bradley, D. D. C.; Dos Santos, D. A.; Brédas, J. L.; Lögdlund, M. *Nature* **1999,** *397*, 121–128; (b) Bernius, M. T.; Inbasekaran, M.; O'Brien, J.; Wu, W. *Adv. Mater.* **2000,** *12*, 1737–1750; (c) Akcelrud, L. *Prog. Polym. Sci.* **2003,** *28*, 875–962.

5 (a) Takiguchi, T.; Park, D. H.; Ueno, H.; Yoshino, K.; Sugimoto, R. *Synth. Met.* **1987,** *17*, 657–662; (b) Braun, D.; Heeger, A. J. *Appl. Phys. Lett.* **1991,** *58*, 1982–1984.

6 (a) Kraft, A.; Burn, P. L.; Holmes, A. B.; Bradley, D. D. C.; Friend, R. H.; Martens, J. H. F. *Synth. Met.* **1993,** *57*, 4163–4167; (b) Antoniadis, H.; Abkowitz, M. A.; Hsieh, B. R. *Appl. Phys. Lett.* **1994,** *65*, 2030–2032.

7 (a) Meyer, H.; Haarer, D.; Naarmann, H.; Hörhold, H. H. *Phys. Rev. B* **1995,** *52*, 2587–2598; (b) Blom, P. W. M.; de John, M. J. M.; Vleggaar, J. J. M. *Appl. Phys. Lett.* **1996,** *68*, 3308–3310.

8 (a) Yang, Y.; Pei, Q.; Heeger, A. J. *J. Appl. Phys.* **1996,** *79*, 934–939; (b) Wang, Y. Z.; Gebler, D. D.; Spry, D. J.; Fu, D. K.; Swager, T. M.; MacDiarmid, A. G.; Epstein, A. J. *IEEE Trans. Electron Devices* **1997,** *44*, 1263–1268.

9 (a) Li, X.-C.; Grimsdale, A. C.; Cervini, R.; Holmes, A. B.; Moratti, S. C.; Yong, T. M.; Grüner, J.; Friend, R. H. *ACS Symp. Ser.* **1997,** *672*, 322–344; (b) Meng, H.; Yu, W. L.; Huang, W. *Macromolecules* **1999,** *32*, 8841–8847; (c) Martens, H. C. F.; Huiberts, J. N.; Blom, P. W. M. *Appl. Phys. Lett.* **2000,** *77*, 1852–1854.

10 Adachi, C.; Tsutsui, T.; Saito, S. *Appl. Phys. Lett.* **1989,** *55*, 1489–1491.

11 (a) Brown, A. R.; Bradley, D. D. C.; Burroughes, J. H.; Friend, R. H.; Greenham, N. C.; Burn, P. L.; Holmes, A. B.; Kraft, A. *Appl. Phys. Lett.* **1992,** *61*, 2793–2795; (b) Greenham, N. C.; Moratti, S. C.; Bradley, D. D. C.; Friend, R. H.; Holmes, A. B. *Nature* **1993,** *365*, 628–630.

12 (a) Parker, I. D.; Pei, Q.; Marrocco, M. *Appl. Phys. Lett.* **1994,** *65*, 1272–1274; (b) Son, S.; Dodabalapur, A.; Lovinger, A. J.; Galvin, M. E. *Science* **1995,** *269*, 376–378.

13 (a) Zhang, Y.-D.; Hreha, R. D.; Jabbour, G. E.; Kippelen, B.; Peyghambarian, N.; Marder, S. R. *J. Mater. Chem.* **2002,** *12*, 1703–1708; (b) Bacher, E.; Bayerl, M.; Rudati, P.; Reckefuss, N.; Muller, C. D.; Meerholz, K.; Nuyken, O. *Macromolecules* **2005,** *38*, 1640–1647.

14 (a) Lee, S.; Lee, B.; Kim, B. J.; Park, J.; Yoo, M.; Bae, W. K.; Char, K.; Hawker, C. J.; Bang, J.; Cho, J. *J. Am. Chem. Soc.* **2009,** *131*, 2579–2587; (b) Akhrass, S. A.; Gal, F.; Damiron, D.; Alcouffe, P.; Hawker, C. J.; Cousin, F.; Carrot, G.; Drockenmuller, E. *Soft Matter* **2009,** *5*, 586–592.

15 (a) Zhu, K.; Iacono, S. T.; Budy, S. M.; Jin, J.; Smith, D. W. *J. Polym. Sci. Part A: Polym. Chem.* **2010,** *48*, 1887–1893; (b) Akhrass, S. A.; Damiron, D.; Carrot, G.; Drockenmuller, E. *J. Polym. Sci. Part A: Polym. Chem.* **2010,** *48*, 3888–3895.

16 (a) Chen, J. P.; Klaerner, G.; Lee, J. I.; Markiewicz, D.; Lee, V. Y.; Miller, R. D.; Scott, J. C. *Synth. Met.* **1999,** *107*, 129–135; (b) Liu, S.; Jiang, X.; Ma, H.; Liu, M. S.; Jen, A. K. Y. *Macromolecules* **2000,** *33*, 3514–3517; (c) Jiang, X. Z.; Liu, S.; Liu, M. S.; Herguth, P.; Jen, A. K. Y.; Fong, H.; Sarikaya, M. *Adv. Funct. Mater.* **2002,** *12*, 745–751.

17 (a) Niu, Y.-H.; Liu, M. S.; Ka, J.-W.; Jen, A. K. Y. *Appl. Phys. Lett.* **2006,** *88*, 093505; (b) Paul, G. K.; Mwaura, J.; Argun, A. A.; Taranekar, P.; Reynolds, J. R. *Macromolecules* **2006,** *39*, 7789–7792.

18 (a) Niu, Y.-H.; Liu, M. S.; Ka, J.-W.; Bardeker, J.; Zin, M. T.; Schofield, R.; Chi, Y.; Jen, A. K.-Y. *Adv. Mater.* **2007,** *19*, 300–304; (b) Cheng, Y.-J.; Liu, M. S.; Zhang, Y.; Niu, Y.; Huang, F.; Ka, J.-W.; Yip, H.-L.; Tian, Y.; Jen, A. K.-Y. *Chem. Mater.* **2008,** *20*, 413–422; (c) Liu, M. S.; Niu, Y.-H.; Ka, J.-W.; Yip, H.-L.; Huang, F.; Luo, J.; Kim, T.-D.; Jen, A. K. Y. *Macromolecules* **2008,** *41*, 9570–9580.

19 (a) Lim, B.; Hwang, J.-T.; Kim, J. Y.; Ghim, J.; Vak, D.; Noh, Y.-Y.; Lee, S.-H.; Lee, K.; Heeger, A. J.; Kim, D.-Y. *Org. Lett.* **2006,** *8*, 4703–4706; (b) Krishnan, R. S.; Mackay, M. E.; Duxbury, P. M.; Pastor, A.; Hawker, C. J.; Van Horn, B.; Asokan, S.; Wong, M. S. *Nano. Lett.* **2007,** *7*, 484–489.

20 (a) Kreyenschmidt, M.; Klaerner, G.; Fuhrer, T.; Ashenhurst, J.; Karg, S.; Chen, W. D.; Lee, V. Y.; Scoot, J. C.; Miller, R. D. *Macromolecules* **1998,** *31*, 1099–1103; (b) Grice, A. W.; Bradley, D. D. C.; Bernius, M. T.; Inbasekaran, M.; Wu, W. W.; Woo, E. P. *Appl. Phys. Lett.* **1998,** *73*, 629–631.

21 (a) Scherf, U.; List, E. J. W. *Adv. Mater.* **2002,** *14*, 477–487; (b) Becker, S.; Ego, C.; Grimsdale, A. C.; List, E. J. W.; Marsitzky, D.; Pogantsch, A.; Setayesh, S.; Leising, G.; Müllen, K. *Synth. Met.* **2002,** *125*, 73–80.

22 (a) Babel, A.; Jenekhe, S. A. *Macromolecules* **2003,** *36*, 7759–7764; (b) Cho, N. S.; Hwang, D.-H.; Jung, B.-J.; Lim, E.; Lee, J.; Shim, H.-K. *Macromolecules* **2004,** *37*, 5265–5273.

23 (a) Bellmann, E.; Shaheen, S. E.; Grubbs, R. H.; Marder, S. R.; Kippelen, B.; Peyghambarian, N. *Chem. Mater.* **1999,** *11*, 399–407; (b) Yamamori, A.; Adachi, C.; Koyama, T.; Taniguchi, Y. *Appl Phys. Lett.* **1998,** *72*, 2147–2149; (c) Mitschke, U.; Bäuerle, P. *J. Mater. Chem.* **2000,** *10*, 1471–1507; (d) Ego, C.; Grimsdale, A. C.; Uckert, F.; Yu, G.; Srdanov, G.; Müllen, K. *Adv. Mater.* **2002,** *14*, 809–811.

24 (a) Wu, C.-S.; Chen, Y. *Macromolecules* **2009,** *42*, 3729–3737; (b) Wu, C.-S.; Chen, Y. *J. Mater. Chem.* **2010,** *20*, 7700–7709.

25 (a) Xu, W.; Peng, B.; Chen, J.; Liang, M.; Cai, F. *J. Phys. Chem. C* **2008,** *112*, 874–880; (b) Paul, G. K.; Mwaura, J.; Argun, A. A.; Taranekar, P.; Reynolds, J. R. *Macromolecules* **2006,** *39*, 7789–7792.

26 (a) Wu, C.-S.; Chen, Y. *J. Polym. Sci. Part A: Polym. Chem.* **2010,** *48*, 5727–5736; (b) Wu, C.-S.; Lee, S.-L.; Chen, Y. *J. Polym. Sci. Part A: Polym. Chem.* **2011,** *49*, 3099–3108; (c) Wu, C.-S.; Chen, Y. *J Polym Sci Part A: Polym Chem* **2011,** *49*, 3928–3938.

27 (a) Malliaras, G. G.; Salem, J. R.; Brock, P. J.; Scott, C. *Phys. Rev. B* **1998,** *58*, 13411; (b) Martens, H. C. F.; Brom, H. B.; Blom, P. W. M. *Phys. Rev. B* **1999,** *60*, 8489; (c) Chu, T.-Y.; Song, O.-K. *Appl. Phys. Lett.* **2007,** *90*, 203512.

28 (a) Lebedev, E.; Dittrich, Th.; Petrova-Koch, V.; Karg, S.; Brütting, W. *Appl. Phys. Lett.* **1997,** *71*, 2686–2688; (b) Geens, W.; Shaheen, S. E.; Wessling, B.; Brabec, C. J.; Poortmans, J.; Sariciftci, N. S. *Org. Electron.* **2002,** *3*, 105–110; (c) Inigo, A. R.; Chang, C. C.; Fann, W.; White, J. D.; Huang, Y.-S.; Jeng, U.-S.; Sheu, H. S.; Peng, K.-Y.; Chen, S.-A. *Adv. Mater.* **2005,** *17*, 1835–1838; (d) Inigo, A. R.; Huang, Y.-F.; White, J. D.; Huang, Y.-S.; Fann, W. S.; Peng, K.-Y.; Chen, S.-A. *J. Chin. Chem. Soc.* **2010,** *57*, 459–468.

29 Coulson, D. R.; Satek, L. C.; Grim, S. O. *Inorg. Synth.* **1972,** *13*, 121–124.